

# Numerical Investigation of an Adaptive Vibration Absorber Using Shape Memory Alloys

MARCELO A. SAVI,<sup>1,\*</sup> ALINE S. DE PAULA<sup>2</sup> AND DIMITRIS C. LAGOUDAS<sup>3</sup>

<sup>1</sup>*COPPE, Department of Mechanical Engineering, Universidade Federal do Rio de Janeiro, PO Box 68.503, 21.941.972, Rio de Janeiro, RJ, Brazil*

<sup>2</sup>*Department of Mechanical Engineering, Universidade de Brasília, 70.910.900, Brasília, DF, Brazil*

<sup>3</sup>*Department of Aerospace Engineering, Texas A&M University, 77843-3409, College Station, Texas, USA*

**ABSTRACT:** The tuned vibration absorber (TVA) is a well-established passive vibration control device for achieving vibration reduction of a primary system subjected to external excitation. This contribution deals with the non-linear dynamics of an adaptive tuned vibration absorber (ATVA) with a shape memory alloy (SMA) element. Initially, a single-degree of freedom oscillator with an SMA element is analyzed showing the general characteristics of its dynamical response. Then, the analysis of an ATVA with an SMA element is carried out. Initially, small amplitude vibrations are considered in such a way that the SMA element does not undergo a stress-induced phase transformation. Under this assumption, the SMA influence is only caused by stiffness changes corresponding to temperature-induced phase transformation. Afterwards, the influence of the hysteretic behavior due to stress-induced phase transformation is considered. A proper constitutive description is employed in order to capture the general thermomechanical aspects of the SMAs. The hysteretic behavior introduces complex characteristics to the system dynamics but also changes the absorber response allowing vibration reduction in different frequency ranges. Numerical simulations establish comparisons of the ATVA results with those obtained from the classical TVA.

*Key Words:* control, vibration absorber, shape memory alloys, non-linear dynamics, hysteresis.

## INTRODUCTION

VIBRATION control is an essential task in engineering being related to different applications. The main goal is vibration reduction by employing either active or passive procedures. The tuned vibration absorber (TVA) is a well-established passive vibration control device for achieving reduction in the vibration of a primary system subject to external excitation (Meirovitch, 1986; Inman, 1989). The TVA consists of a secondary oscillatory system that once attached to the primary system is capable of absorbing vibration energy from the primary system. By tuning the natural frequency of the TVA to a chosen excitation frequency, one produces an attenuation of the primary system vibration amplitude for this specific forcing frequency. An alternative for systems where the forcing frequency varies or has a kind of uncertainty is the concept of an adaptive tuned vibration absorber (ATVA). This device is an adaptive-passive vibration control similar to a TVA but

with adaptive elements that can be used to change the tuned condition (Brennan, 2006; Ibrahim, 2008).

The remarkable properties of shape memory alloys (SMAs) are attracting technological interest in several science and engineering fields and numerous applications have been developed exploiting singular characteristics of these alloys (Machado and Savi, 2003; Paiva and Savi, 2006; Lagoudas, 2008). In terms of applied dynamics, SMAs are being used in order to explore adaptive dissipation associated with hysteresis loop and the mechanical property changes due to phase transformation (van Humbeeck, 2003; Savi et al., 2008). Moreover, the dynamical response of systems with SMA actuators presents a unique dynamical behavior due to their intrinsic non-linear characteristic, presenting periodic, quasi-periodic, and chaotic responses (Savi and Pacheco, 2002; Machado et al., 2003, 2009; Bernardini and Rega, 2005; Savi et al., 2008). Recently, SMA constraints have been used for vibration reduction since it is expected that the high dissipation capacity of SMA changes the system response producing less complex behaviors (Sitnikova et al., 2008, 2010; Santos and Savi, 2009).

In this regard, SMAs have been used in a number of approaches to passive structural vibration control

\*Author to whom correspondence should be addressed.  
E-mail: savi@mecanica.ufrj.br  
Figure 12 appears in color online: <http://jim.sagepub.com>

(Salichs et al., 2001; Saadat et al., 2002; Lagoudas et al., 2004; Machado et al., 2009). SMA characteristics motivate the concept of an ATVA that is able to change its stiffness depending on the SMA element's temperature (Elahinia et al., 2005). This property allows one to attenuate primary system vibration amplitudes not only for one specific forcing frequency, as occurs with the TVA, but for a range of frequencies.

Williams et al. (2002) presented an adaptive–passive vibration controller using SMA elements in an ATVA. The device is manually tuned in order to achieve attenuation of vibration of the primary system across a range of frequencies. Williams et al. (2005) showed a continuously tuned SMA–ATVA as a novel adaptive–passive vibration control device. The same idea was used in Rustighi et al. (2005a) that treated an SMA–ATVA made from a beam-like structure supported in its center. Numerical and experimental tests were performed showing that a change in the stiffness of the ATVA can be obtained by a temperature variation, which changes the Young's modulus, resulting in a variation of the tuning frequency. Rustighi et al. (2005b) presented control algorithms for real-time adaptation of this SMA–ATVA device both theoretically and experimentally. In general, the literature discusses the effect of property change due to the temperature-induced phase transformation in SMA–ATVA devices, but does not treat the influence of the hysteretic behavior due to stress-induced phase transformation.

This article deals with the non-linear dynamics of an SMA–ATVA. Initially, a single-degree of freedom (1DOF) oscillator with an SMA element is analyzed showing the general characteristics of its dynamical response. Then, the analysis of an SMA–ATVA is carried out. This analysis starts by considering small amplitude vibrations in a way that the SMA element does not exhibit stress-induced phase transformation. Under this assumption, the SMA's influence is only due to stiffness changes. This kind of analysis is the most common in literature and is followed by an investigation concerning the influence of the hysteretic behavior due to stress-induced phase transformation by considering a proper description of the thermomechanical behavior of SMAs. All results from the SMA–ATVA are compared with those obtained from the classical TVA, establishing a proper contrast between the devices and their capacity to promote vibration reduction.

This article is divided into five sections. After this introduction, second section discusses the constitutive model employed to describe the thermomechanical behavior of SMAs. Third section presents an analysis of a 1DOF SMA oscillator discussing some important aspects of the SMA dynamical response. A discussion of the vibration absorber dynamics is presented in the fourth section, investigating the classical TVA and an ATVA with an SMA element. The analysis of the

adaptive TVA is treated by considering either temperature-induced or stress-induced phase transformations. The influence of the stress-induced hysteretic behavior is analyzed establishing how it can be useful for vibration reduction. Finally, conclusions are highlighted in the last section.

## CONSTITUTIVE MODEL

The thermomechanical behavior of SMAs may be modeled either by microscopic or macroscopic phenomenological points of view. Its description is the objective of numerous research efforts that try to contemplate all behavior details (Paiva and Savi, 2006; Lagoudas, 2008). Here, a constitutive model that is built upon the Fremond's model and previously presented by Oliveira et al. (2010), Aguiar et al. (2010), Paiva et al. (2005), Savi and Paiva (2005), Baêta-Neves et al. (2004), and Savi et al. (2002) is employed. This model considers different material properties for each phase and four macroscopic phases for the description of the SMA behavior. Therefore, besides the total strain,  $\varepsilon$ , and temperature,  $T$ , it is necessary to define four internal variables that represent the volume fraction of each macroscopic phase:  $\beta_1$  and  $\beta_2$ , related to detwinned martensites, respectively associated with tension and compression,  $\beta_3$  that represents the volume fraction of austenite, and  $\beta_4$  that represents the volume fraction of twinned martensite. Since there is a constraint criterion based on phase coexistence,  $\beta_1 + \beta_2 + \beta_3 + \beta_4 = 1$ , it is possible to use only three variables and the thermomechanical behavior of the SMA is described by the following set of equations:

$$\sigma = E\varepsilon + [E\alpha_h + \alpha](\beta_2 - \beta_1) - \Omega(T - T_0) \quad (1)$$

$$\dot{\beta}_1 = \frac{1}{\eta_1} \{ \alpha\varepsilon + \Lambda_1(T) + (2\alpha\alpha_h + E\alpha_h^2)(\beta_2 - \beta_1) + \alpha_h[E\varepsilon - \Omega(T - T_0)] - \partial_{\beta_1} J_\pi \} + \partial_{\dot{\beta}_1} J_\chi \quad (2)$$

$$\dot{\beta}_2 = \frac{1}{\eta_2} \{ -\alpha\varepsilon + \Lambda_2(T) - (2\alpha\alpha_h + E\alpha_h^2)(\beta_2 - \beta_1) - \alpha_h[E\varepsilon - \Omega(T - T_0)] - \partial_{\beta_2} J_\pi \} + \partial_{\dot{\beta}_2} J_\chi \quad (3)$$

$$\dot{\beta}_3 = \frac{1}{\eta_3} \left\{ -\frac{1}{2}(E_A - E_M)[\varepsilon + \alpha_h(\beta_2 - \beta_1)]^2 + \Lambda_3(T) + (\Omega_A - \Omega_M)(T - T_0)[\varepsilon + \alpha_h(\beta_2 - \beta_1)] - \partial_{\beta_3} J_\pi \right\} + \partial_{\dot{\beta}_3} J_\chi \quad (4)$$

Here,  $\sigma$  is the stress,  $E = E_M + \beta_3(E_A - E_M)$  the elastic modulus while  $\Omega = \Omega_M + \beta_3(\Omega_A - \Omega_M)$  related to thermal expansion coefficient. Note that subscript  $A$  refers to austenitic phase, while  $M$  refers to martensite. Parameters  $\Lambda_1 = \Lambda_2 = \Lambda = \Lambda(T)$  and  $\Lambda_3 = \Lambda_3(T)$  are

associated with phase transformation stress levels. Parameter  $\alpha_h$  defines the horizontal width of the stress–strain hysteresis loop, while  $\alpha$  controls the height of the same hysteresis loop. The terms  $\partial_n J_\pi$  ( $n = \beta_1, \beta_2, \beta_3$ ) are sub-differentials of the indicator function  $J_\pi$  with respect to  $n$ . This indicator function is related to a convex set  $\pi$ , which provides the internal constraints related to the coexistence of phases. With respect to evolution equations of volume fractions,  $\eta_1 = \eta_2 = \eta$  and  $\eta_3$  represent the internal dissipation related to phase transformations. Moreover  $\partial_n J_\chi$  ( $n = \beta_1, \beta_2, \beta_3$ ) are sub-differentials of the indicator function  $J_\chi$  with respect to  $n$ . This indicator function is associated with the convex set  $\chi$ , which establishes conditions for the correct description of internal sub-loops due to incomplete phase transformations. These sub-differentials may be replaced by Lagrange multipliers associated with the mentioned constraints (Savi et al., 2002).

Concerning parameter definitions, temperature dependent relations are adopted for  $\Lambda$  and  $\Lambda_3$  as follows:

$$\Lambda = \begin{cases} -L_0 + \frac{L}{T_M}(T - T_M), & \text{if } T > T_M \\ -L_0, & \text{if } T \leq T_M \end{cases} \quad (5)$$

$$\Lambda_3 = \begin{cases} -L_0^A + \frac{L^A}{T_M}(T - T_M), & \text{if } T > T_M \\ -L_0^A, & \text{if } T \leq T_M \end{cases} \quad (6)$$

Here,  $T_M$  is the temperature below where the martensitic phase becomes stable. Usually, experimental tests provide information of  $M_s$  and  $M_f$ , temperatures of the start and finish of the martensitic formation. This model uses only one temperature that could be an average value or alternatively,  $M_s$  or  $M_f$  values. Moreover,  $L_0$ ,  $L$ ,  $L_0^A$ , and  $L^A$  are parameters related to critical stress for phase transformation.

In order to describe the characteristics of phase transformation kinetics, different values of  $\eta$  and  $\eta_3$  might be considered during loading,  $\eta^L$  and  $\eta_3^L$ , and unloading processes,  $\eta^U$  and  $\eta_3^U$ . For more details about the constitutive model, see Paiva et al. (2005) and Savi and Paiva (2005). All constitutive parameters can be matched from stress–strain tests.

As it is well-known, SMA devices demonstrate time-dependence characteristics which means that their thermomechanical response depends on the loading rate, see for example, Shaw and Kyriakides (1995) and Yoon (2008). The adequate modeling of this time-dependency can be performed by considering the thermomechanical coupling terms in the energy equation. Monteiro et al. (2009) discussed the thermomechanical coupling and rate-dependency in SMAs. The considered constitutive

model has viscous characteristic that allows the description of the thermomechanical coupling avoiding the integration of the energy equation, presenting useful results (Aguilar et al., 2010). Auricchio et al. (2006) explores the same idea showing the difference between a viscous model and a rate-independent model with thermomechanical coupling. Both models have the ability to describe pseudoelastic behavior in SMA wires. This time-dependent aspect can be controlled by the proper choice of model parameters.

## SINGLE-DEGREE OF FREEDOM SHAPE MEMORY OSCILLATOR

Initially, the dynamical behavior of SMAs is analyzed by considering a single-degree of freedom (1DOF) oscillator, which consists of a mass  $m$  attached to a shape memory element of length  $l$  and cross-sectional area  $A$ , and restitution force  $F_R$ . A linear viscous damper, characterized by a viscous coefficient  $c$ , is also considered in order to represent dissipations different from the dissipation associated with the SMA element. Moreover, the system is harmonically excited by a force  $F(t) = F_0 \sin(\omega t)$ . Figure 1 shows an oscillator where the restitution force,  $F_R$ , is provided by a general SMA element.

The equation of motion of this oscillator may be formulated by considering the balance of forces acting on the mass as follows:

$$m\ddot{u} + c\dot{u} + F_R = F_0 \sin(\omega t) \quad (7)$$

where  $F_R = \sigma A$ . The restitution force of the oscillator may be provided by an SMA element described by the constitutive equations presented in the previous section (Paiva et al., 2005). Therefore, the following equation of motion is obtained (Savi et al., 2008):

$$m\ddot{u} + c\dot{u} + \frac{EA}{l}u + (A\alpha + EA\alpha_h)(\beta_2 - \beta_1) - \Omega A(T - T_0) = F_0 \sin(\omega t) \quad (8)$$

where volume fractions evolution  $\beta_1$  and  $\beta_2$  are described by the constitutive model presented in the

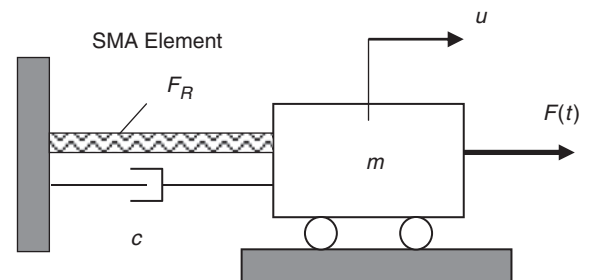


Figure 1. 1DOF oscillator.

preceding section and  $\varepsilon = u/l$ . In order to obtain a dimensionless equation of motion, the system's parameters are defined as follows:

$$\begin{aligned}\delta &= \frac{F_0}{ml\omega_0^2} = \frac{F_0}{E_R A}; & \bar{\Omega} &= \frac{\Omega_R A T_R}{ml\omega_0^2} = \frac{\Omega_R T_R}{E_R}; \\ \bar{\alpha} &= \frac{\alpha A}{ml\omega_0^2} = \frac{\alpha}{E_R}; & \bar{\alpha}_h &= \frac{\alpha_h E_R A}{ml\omega_0^2} = \alpha_h; \\ \omega_0^2 &= \frac{E_R A}{ml}; & \xi &= \frac{c}{m\omega_0}; & \mu_E &= \frac{E}{E_R}; \\ \mu_\Omega &= \frac{\Omega}{\Omega_R}; & \varpi &= \frac{\omega}{\omega_0}\end{aligned}\quad (9)$$

Note that dimensionless parameters and variables are defined considering some reference values for temperature dependent parameters. This is done by assuming a reference temperature,  $T_R$ , where these parameters are evaluated. Therefore, parameters with subscript  $R$  are evaluated at this reference temperature. These definitions allow one to define the following dimensionless variables, respectively related to mass displacement ( $U$ ), temperature ( $\theta$ ), and time ( $\tau$ ):

$$U = \frac{u}{l}; \quad \theta = \frac{T}{T_R}; \quad \tau = \omega_0 t \quad (10)$$

Therefore, the dimensionless equation of motion has the form:

$$\begin{aligned}U'' + \xi U' + \mu_E U + (\bar{\alpha} + \mu_E \bar{\alpha}_h)(\beta_2 - \beta_1) \\ - \mu_\Omega \bar{\Omega}(\theta - \theta_0) = \delta \sin(\varpi \tau)\end{aligned}\quad (11)$$

where derivatives with respect to dimensionless time are represented by ( $' = d(\ )/d\tau$ ).

Besides the non-linear SMA oscillator, an elastic 1DOF oscillator is analyzed by replacing the SMA element by an elastic element where the restitution force is given by  $F_R = ku$  and its natural frequency is  $\omega_L = \sqrt{k/m}$ . The equivalent elastic oscillator is governed by:

$$U'' + \xi U' + \frac{\omega_L^2}{\omega_0^2} U = \delta \sin(\varpi \tau) \quad (12)$$

Note that in the above equation, the rate  $\omega_L^2/\omega_0^2$  appears even though it describes the linear elastic system. This is due to the definition of the dimensionless time,  $\tau = \omega_0 t$ , where  $\omega_0$  is related to the natural frequency of the SMA system. This consideration allows one to establish a proper comparison between the elastic and the SMA systems.

## Numerical Simulation

In order to deal with non-linearities of the SMA oscillator equations of motion, an iterative procedure based on the operator split technique (Ortiz et al.,

1983) is employed. Under this assumption, the fourth-order Runge–Kutta method is used together with the projection algorithm proposed by Savi et al. (2002) to solve the constitutive equations. The solution of the constitutive equations also employs the operator split technique together with an implicit Euler method. The calculation of  $\beta_n$  ( $n = 1, 2, 3$ ) considers that the evolution equations are solved in a decoupled way. At first, the equations (except for the sub-differentials) are solved using an iterative implicit Euler method. If the estimated results obtained for  $\beta_n$  do not satisfy the imposed constraints, the orthogonal projection algorithm pulls their value to the nearest point on the domain's surface (Paiva et al., 2005). On the other hand, the numerical integration of the linear system uses the classical Runge–Kutta approach.

The numerical investigation starts by considering an analysis of the linear system. Values of  $m = 1$ ,  $\omega_L = 0.72\omega_0$ , an excitation frequency of  $\omega = 0.72\omega_0$  and a forcing amplitude  $\delta = 0.01$  are considered. The natural frequency of the linear system is chosen in such way that the resonance frequency occurs in a value where the SMA system presents high oscillation amplitude. Under these conditions, the system presents the well-known resonant response showed in Figure 2 for undamped ( $\xi = 0$ , left side) and damped ( $\xi = 0.05$ , right side) oscillators. The undamped case presents a response where amplitude grows indefinitely while the damped system response tends to stabilize in specific amplitude.

The same 1DOF oscillatory system is now considered, however, the linear elastic element is replaced by an SMA element. The SMA parameters used in numerical simulations are given in Table 1. All simulations are carried out with  $T = 372$  K, a high temperature where austenite is stable for a stress-free state. Moreover, an SMA element with  $A = 1.96 \times 10^{-5} \text{ m}^2$  and  $l = 50 \times 10^{-3} \text{ m}$  is considered and a reference temperature  $T_R = T_M$  is assumed.

Both conditions analyzed for the elastic oscillator are now reproduced for the SMA oscillator. Figures 3 and 4 show displacement time history located on the left and the correspondent stress–strain curve located on the right for the same forcing frequency imposed to the linear system, with and without external viscous damping. In both cases, the hysteretic behavior of the SMA oscillator tends to attenuate the amplitude response when compared to the linear system.

Due to non-linearities, the SMA oscillator response is far more complex than the linear oscillator response. Bernardini and Rega (2005) discussed some aspects related to SMA system resonant conditions. In order to identify some resonant characteristics of the SMA oscillator, non-linear resonant curves are plotted by increasing (up-sweep) and decreasing (down-sweep) forcing frequency. In both situations, the system is

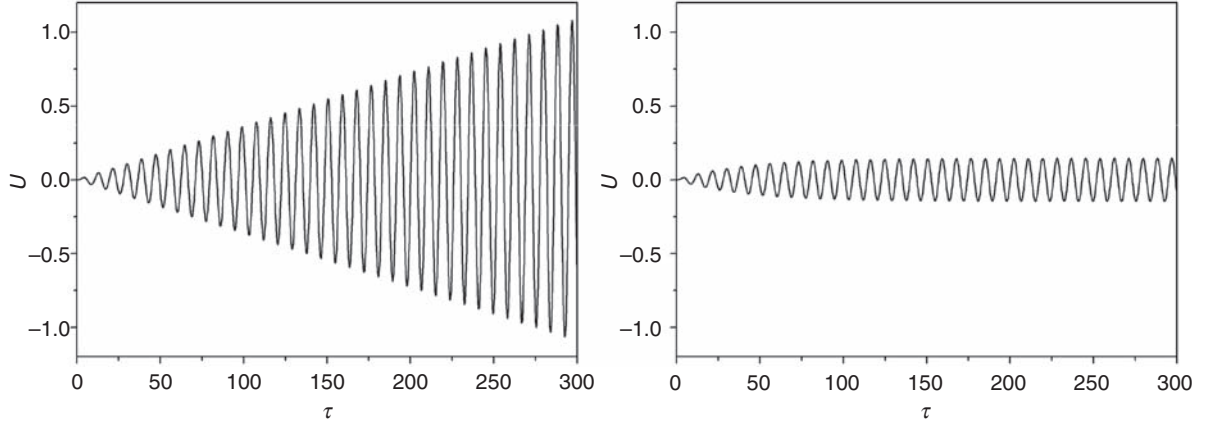


**Figure 2.** Linear system response for  $\omega = 0.72\omega_0$ .  
 Note: Left, undamped oscillator ( $\xi = 0$ ); Right, damped system ( $\xi = 0.05$ ).

**Table 1. SMA parameters.**

$E_A$ (GPa)	$E_M$ (GPa)	$A$ (MPa)	$\alpha_h$	$L_0$ (MPa)	$L$ (MPa)	$L_0^A$ (MPa)	$L^A$ (MPa)
54	42	330	0.048	0.15	41.5	0.63	185
$\Omega_A$ (MPa/K)	$\Omega_M$ (MPa/K)	$T_M$ (K)	$\eta^L$ (MPa.s)	$\eta^U$ (MPa.s)	$\eta_3^L$ (MPa.s)	$\eta_3^U$ (MPa.s)	
0.74	0.17	291.4	1.0	2.7	1.0	2.7	

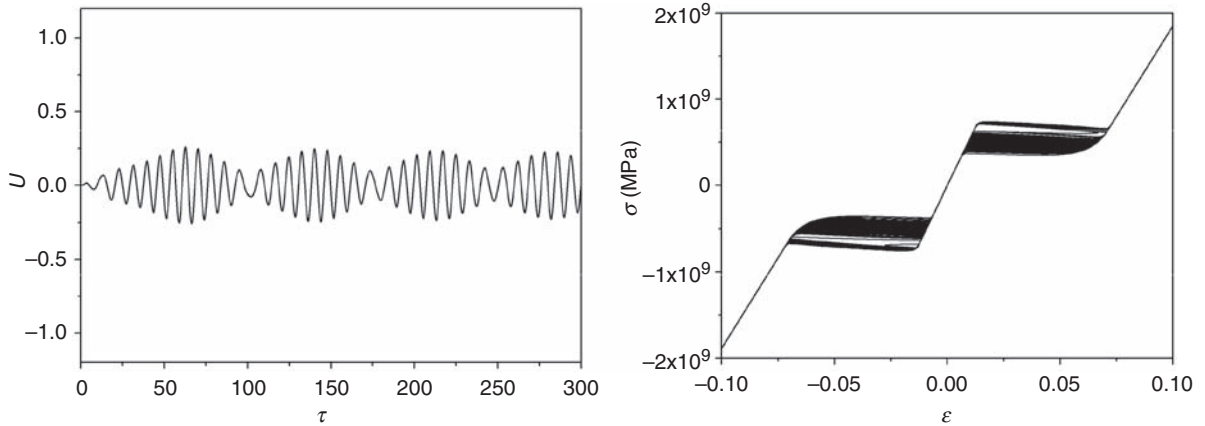


**Figure 3.** SMA oscillator response for  $\omega = 0.72$  and  $\xi = 0$ .  
 Note: Left, time response; Right, stress–strain curve.

numerically integrated assessing the maximum steady state amplitude. Figure 5 shows the maximum amplitudes of the system response as a function of the forcing frequency with different forcing amplitudes:  $\delta = 0.008$  and  $\delta = 0.012$ . It is evident that non-linearities introduce dynamical jumps to the system response and that the variation of forcing amplitude changes the frequency where jumps occur. Moreover, it should be highlighted that the response of the SMA system tends to present smaller vibration amplitude when compared to those obtained by the elastic oscillator. This result shows some aspects of the SMA's dynamical response. The

next section addresses the use of SMA elements in secondary system used in vibration absorbers.

## NON-LINEAR VIBRATION ABSORBERS

The ATVA is an adaptive–passive vibration control device similar to a TVA but with adaptive elements that can be used to change the ATVA tuned condition. The aim of ATVAs with SMA elements (SMA–ATVA) is to attenuate primary system vibration amplitudes, not only for one specific forcing frequency, as occurs with the TVA, but for a range of frequencies exploring the

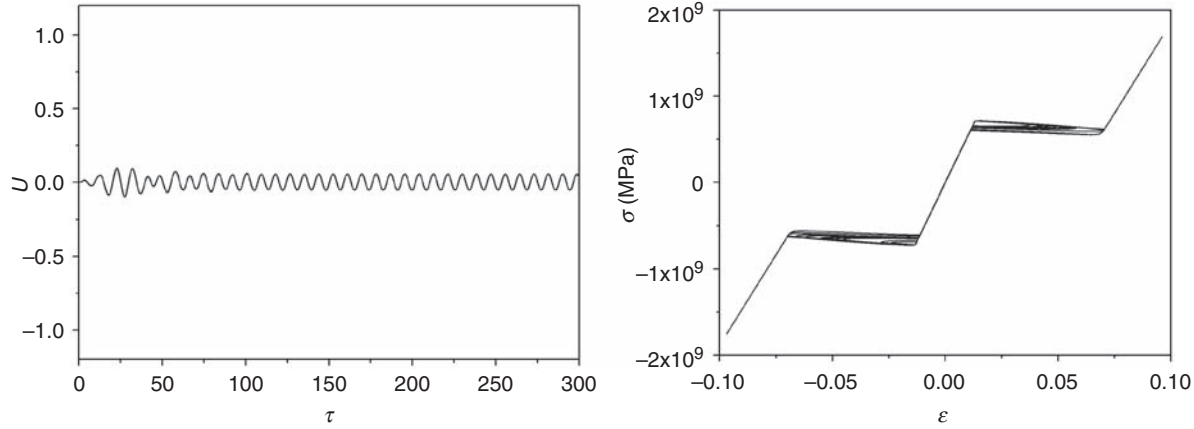


**Figure 4.** SMA oscillator response for  $\varpi = 0.72$  and  $\xi = 0.05$ .  
Note: Left, time response; Right, stress–strain curve.

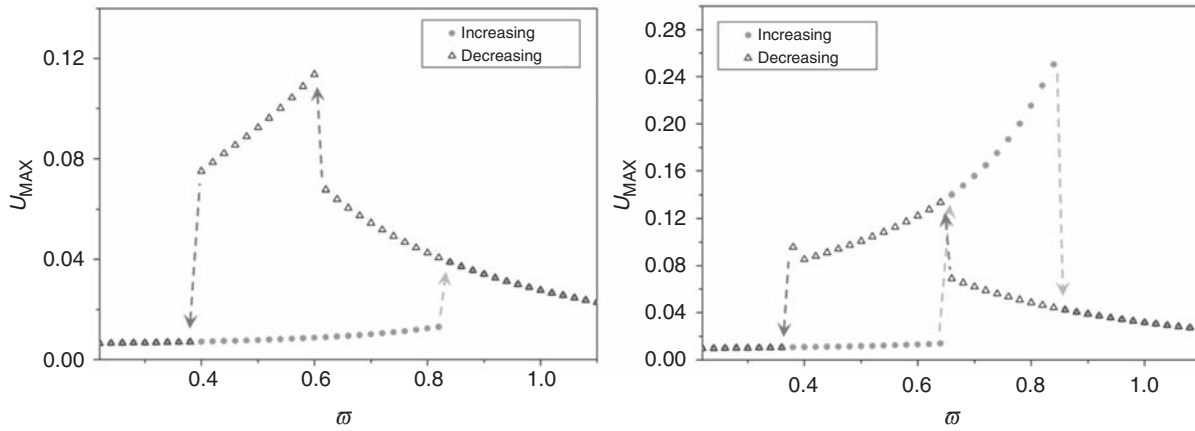


**Figure 5.** Maximum amplitudes response increasing (up-sweep) and decreasing (down-sweep) forcing frequency for different forcing amplitudes.  
Note: Left,  $\delta = 0.008$ ; Right,  $\delta = 0.012$ .

temperature dependent characteristic of the SMAs. This section investigates the SMA–ATVA dynamics by establishing a comparison between two different absorbers: a TVA and an SMA–ATVA. The analysis of the SMA–ATVA is done by considering two different approaches. The first investigates small amplitude response that does not induce stress-induced phase transformation, which is the classical approach in literature. On the other hand, the second approach considers stress-induced phase transformations and therefore, is associated with energy dissipation due to hysteretic behavior. In addition, temperature variations are of concern, assuming the steady state response. Therefore, different, constant temperatures are treated in such a way that slow varying temperatures are of interest.

Figure 6 shows a 2DOF system that represents a primary system, subsystem  $(m_1, c_1, k_1)$ , that is harmonically excited by an external force  $F = F_0 \sin(\omega t)$  and whose vibration amplitudes wish to be reduced by using a secondary system that consists of a concentrated mass,  $m_2$ ,

attached to a viscous damper with coefficient,  $c_2$ , and to an element with restoring force  $F_R$ . This element could be an SMA element with length  $l$  and transversal section area  $A$ , defining an SMA–ATVA system or a linear elastic element defining a classical TVA. Once again, all dissipation mechanisms of the system are represented by the viscous damping coefficients ( $c_1$  and  $c_2$ ) except for the hysteretic dissipation of the SMA element.

Both the classical TVA and the SMA–ATVA systems may be described by the following equations of motion:

$$\begin{cases} m_1 \ddot{u}_1 + (c_1 + c_2) \dot{u}_1 - c_2 \dot{u}_2 + k u_1 - F_R = F_0 \sin(\omega t) \\ m_2 \ddot{u}_2 - c_2 \dot{u}_1 + c_2 \dot{u}_2 + F_R = 0 \end{cases} \quad (13)$$

The description of the restitution force depends on the kind of absorber. The SMA–ATVA has a restitution force  $F_R$  that is described by the constitutive equation presented in section ‘Constitutive model.’ Therefore, the

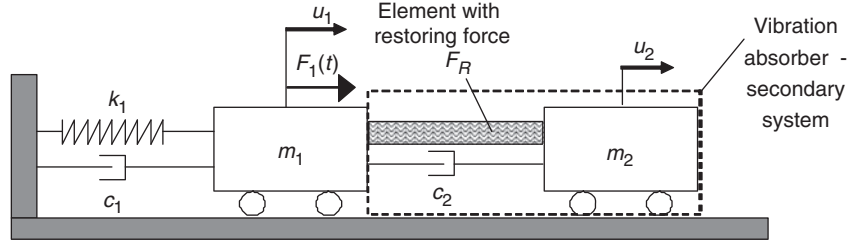


Figure 6. Vibration absorber connected to a primary system.

SMA–ATVA system has the following equations of motion together with the SMA constitutive equation:

$$\begin{cases} m_1 \ddot{u}_1 + (c_1 + c_2) \dot{u}_1 - c_2 \dot{u}_2 + k u_1 - \frac{EA}{l} (u_2 - u_1) \\ - (A\alpha + EA\alpha_h)(\beta_2 - \beta_1) + \\ + \Omega A(T - T_0) = F_0 \sin(\omega t) \\ m_2 \ddot{u}_2 - c_2 \dot{u}_1 + c_2 \dot{u}_2 + \frac{EA}{l} (u_2 - u_1) \\ + (A\alpha + EA\alpha_h)(\beta_2 - \beta_1) - \Omega A(T - T_0) = 0 \end{cases} \quad (14)$$

In order to obtain dimensionless equations of motion, system's parameters are defined as follows:

$$\begin{aligned} \omega_{01}^2 &= \frac{k}{m_1}; & \omega_{02}^2 &= \frac{E_R A}{m_2 l}; & \xi_1 &= \frac{c_1}{m_1 \omega_{02}}; & \xi_2 &= \frac{c_2}{m_2 \omega_{02}}; \\ \gamma_\omega &= \frac{\omega_{01}^2}{\omega_{02}^2}; & \gamma_m &= \frac{m_2}{m_1}; & \bar{\alpha} &= \frac{\alpha A}{m_2 l \omega_{02}^2} = \frac{\alpha}{E_R}; \\ \bar{\alpha}_h &= \frac{\alpha_h E_R A}{m_2 l \omega_{02}^2} = \alpha_h; & \delta &= \frac{F_0}{m_1 l \omega_{02}^2} = \frac{m_2}{m_1} \frac{F_0}{E_R A}; \\ \bar{\Omega} &= \frac{\Omega_R A T_R}{m_2 l \omega_{02}^2} = \frac{\Omega_R T_R}{E_R}; & \mu_E &= \frac{E}{E_R}; & \mu_\Omega &= \frac{\Omega}{\Omega_R}; \\ \varpi &= \frac{\omega}{\omega_{02}} \end{aligned} \quad (15)$$

These definitions allow one to define the following dimensionless variables, respectively related to mass displacements ( $U_1, U_2$ ), temperature ( $\theta$ ) and time ( $\tau$ ):

$$U_1 = \frac{u_1}{l}; \quad U_2 = \frac{u_2}{l}; \quad \theta = \frac{T}{T_R}; \quad \tau = \omega_{02} t. \quad (16)$$

Therefore:

$$\begin{cases} U_1'' + (\xi_1 + \gamma_m \xi_2) U_1' - \gamma_m \xi_2 U_2' + \gamma_\omega U_1 \\ + \gamma_m [-\mu_E (U_2 - U_1) - (\bar{\alpha} + \mu_E \bar{\alpha}_h)(\beta_2 - \beta_1) \\ + \mu_\Omega \bar{\Omega} (\theta - \theta_0)] = \delta \sin(\varpi \tau) \\ U_2'' - \xi_2 U_1' + \xi_2 U_2' + \mu_E (U_2 - U_1) \\ + (\bar{\alpha} + \mu_E \bar{\alpha}_h)(\beta_2 - \beta_1) - \mu_\Omega \bar{\Omega} (\theta - \theta_0) = 0 \end{cases} \quad (17)$$

The TVA has a linear restitution force,  $F_R = k_L(u_2 - u_1)$ , that results in the following

dynamical system expressed as dimensionless equations as follows:

$$\begin{cases} U_1'' + \left( \xi_1 + \frac{m_2}{m_1} \xi_2 \right) U_1' - \frac{m_2}{m_1} \xi_2 U_2' + \left( \frac{\omega_{L1}^2}{\omega_{02}^2} + \frac{m_2}{m_1} \frac{\omega_{L2}^2}{\omega_{02}^2} \right) U_1 \\ - \frac{m_2}{m_1} \frac{\omega_{L2}^2}{\omega_{02}^2} U_2 = \delta \sin(\varpi \tau) \\ U_2'' - \xi_2 U_1' + \xi_2 U_2' - \frac{\omega_{L2}^2}{\omega_{02}^2} U_1 + \frac{\omega_{L2}^2}{\omega_{02}^2} U_2 = 0 \end{cases} \quad (18)$$

where  $\omega_{L1}^2 = \frac{k_1}{m_1}$  and  $\omega_{L2}^2 = \frac{k_L}{m_2}$ , respectively representing the isolated natural frequencies of primary and secondary systems. As presented in the 1DOF system, we are assuming a dimensionless time  $\tau = \omega_{02} t$  for elastic and SMA systems and therefore, the equations of motion present rates  $\omega_{L2}^2/\omega_{02}^2$  and  $\omega_{L1}^2/\omega_{02}^2$ .

This article considers a primary system with  $m_1 = 5$  kg and  $k_1 = 5k_L$ . A critical case where the primary system is under resonant conditions is assumed. Initially, the TVA is of concern and the mass and the stiffness values are chosen in such a way that the natural frequency of the primary system is the same as the 1DOF oscillator considered in the last section:  $m_1/m_2 = 5$  and  $k_L = 0.72^2 \times E_R A/l$ . Figure 7 shows the response of the TVA primary system showing the maximum amplitudes as a function of the forcing frequency with  $\delta = 0.01$ . Two different damping coefficients are analyzed representing an undamped system ( $\xi_1 = \xi_2 = 0$ ) and a damped system ( $\xi_1 = \xi_2 = 0.2$ ). These results are compared with the 1DOF oscillator response. It can be observed that for  $\varpi = 0.72$ , critical resonant situation for the 1DOF oscillator, the absorber reduces the amplitude of the primary system response. Nevertheless, the new degree of freedom related to the secondary system introduces two resonant frequencies, identified in  $\omega_1 = 0.58\varpi$  and  $\omega_2 = 0.9\varpi$ . The undamped system presents amplitudes that increase indefinitely in these frequencies while the damping tends to limit the amplitude increase as shown in Figure 7.

The forthcoming analysis discusses the SMA–ATVA, showing how it can be useful for vibration reduction. Two different analyses are developed by exploring the hysteresis loop related to stress-induced phase

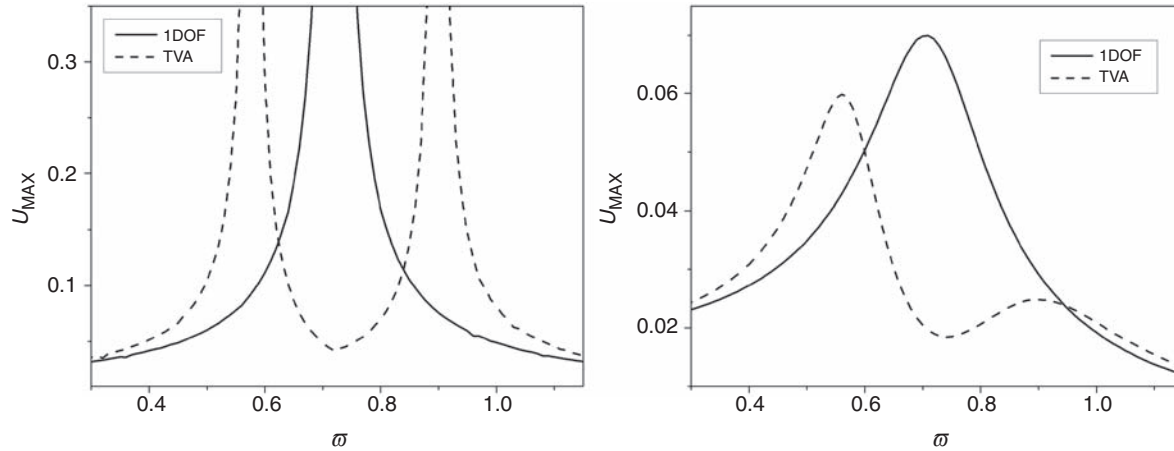


**Figure 7.** Maximum amplitudes response of the 1DOF linear oscillator and of the TVA primary system with  $\delta=0.01$ . Note: Left,  $\xi_1 = \xi_2 = 0$ ; Right,  $\xi_1 = \xi_2 = 0.2$ .

transformations and the classical approach where only the stiffness change is considered. In addition, temperature variations are of concern, assuming the steady state response. Therefore, different, constant temperatures are treated in such a way that slow varying temperatures are of interest. Initially, small amplitude movement is investigated and, therefore, the SMA element does not present stress-induced phase transformations. Under this condition, it is possible to alter the absorber natural frequencies due to the change of the element's stiffness caused by temperature-induced phase transformations. In this regard, two different ranges of temperatures are considered: temperatures where martensite is stable (below  $T_M$ ), and temperatures where austenite is stable (higher than  $T_A = 307.5$  K). The same characteristics of the primary oscillator ( $m_1 = 5$  kg,  $k = 5 \times 0.72^2 \times E_R A / l$ ) are assumed and the vibration absorber has  $m_2 = 1$  kg with an SMA element with the same characteristics discussed in the previous section ( $A = 1.96 \times 10^{-5}$  m<sup>2</sup> and  $l = 50 \times 10^{-3}$  m). Figure 8 shows a comparison between system responses for two different temperatures, showing that it is possible to change the range of frequencies where the primary system amplitude reduction is achieved by changing the temperature. This kind of behavior increases the frequency range where the ATVA can be efficiently used, which is an essential advantage when compared to the elastic TVA.

Although temperature-induced phase transformations can provide flexibility to the SMA-ATVA response, when compared to the classical TVA, the system response may be better explored by assuming large amplitudes of the SMA element that causes stress-induced phase transformations related to hysteretic behavior. The following analysis explores both temperature-induced phase transformation variation and hysteretic behavior due to stress-induced phase transformations as well.

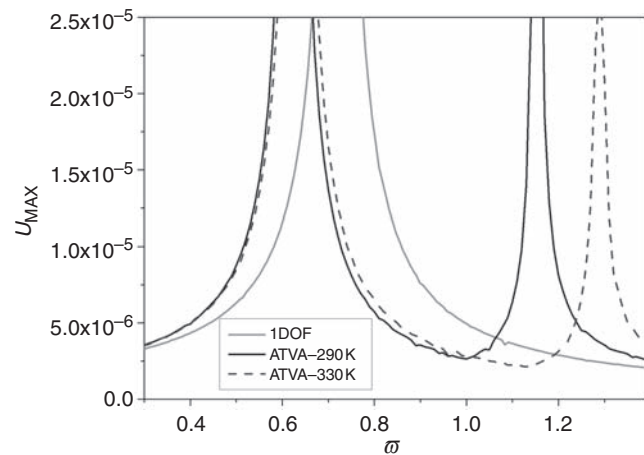


**Figure 8.** SMA-ATVA primary system maximum amplitudes response for different temperatures.

### SMA-ATVA Exploring Stress-Induced Hysteresis Loop

We now consider the general application of the SMA-ATVA where the amplitudes are no longer limited to small oscillations. Under this new condition, stress-induced phase transformations occur corresponding to the hysteresis loop. This behavior is related to strong non-linearities that are usually associated with complex responses. The analysis is focused on the influence of temperature on the system response, but considering just high temperatures, which means that the SMA element is initially at austenitic phase. Figure 9 shows the SMA element numerical stress-strain curve at 340 and 540 K, showing typical pseudoelastic behavior for high temperatures. Note that the increase in temperature causes the increase of the critical stress level where phase transformation begins to occur. Therefore, we can understand that the increase in temperature is related to the higher position of the hysteresis loop in the

stress–strain space, and this behavior is useful for vibration isolation purposes.

The system response is now analyzed in order to verify the influence of temperature variation on vibration reduction. The previous temperatures are of concern

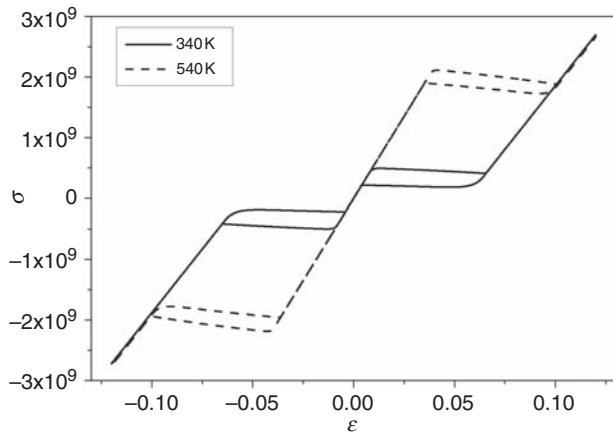


Figure 9. Stress–strain curve for different temperatures.

(340 and 540 K) with parameters  $\varpi = 0.58$ ,  $\delta = 0.0075$ ,  $\xi_1 = \xi_2 = 0.1$ . Figure 10 shows the displacement time history of the primary system (left panel) and the stress–strain curve of the SMA element (right panel). Under these conditions, the SMA element does not present phase transformation and, therefore, the amplitudes is not enough to pass through the hysteresis loop. This kind of behavior makes this response similar to the elastic TVA. Decreasing the temperature to  $T = 340$  K, the hysteresis loop tends to be in a lower position on the stress–strain space as shown in Figure 9. Therefore, the dynamical response of the system starts to dissipate energy due to the hysteresis loop and this large amount of energy dissipation tends to reduce the vibration amplitudes of the primary system. Figure 11 shows the system response represented by the displacement time history of the primary system and the stress–strain curve of the SMA element, confirming the expected behavior.

Although we can achieve a more efficient vibration reduction due to hysteretic energy dissipation, dynamical jumps can make the system response different.

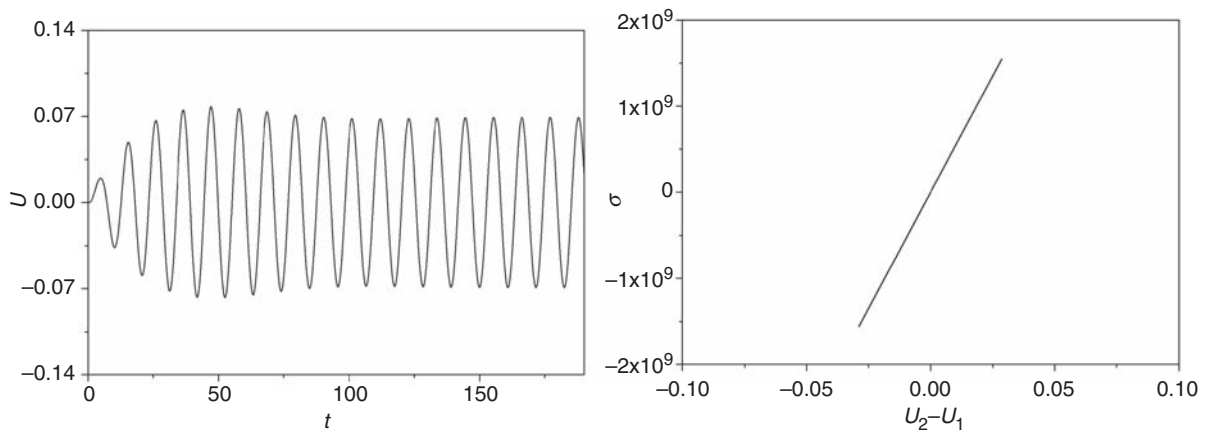


Figure 10. Primary system time response and stress–strain curve at  $T = 540$  K.

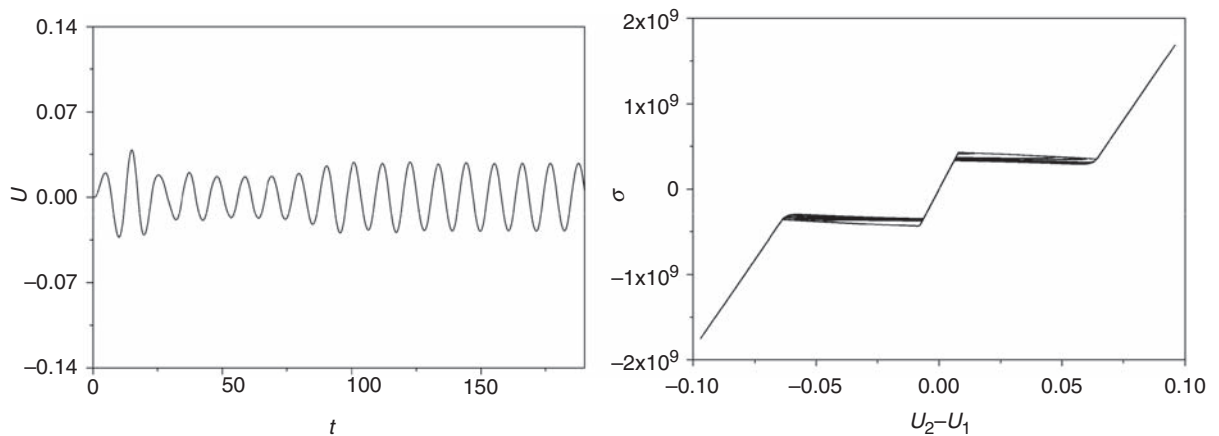
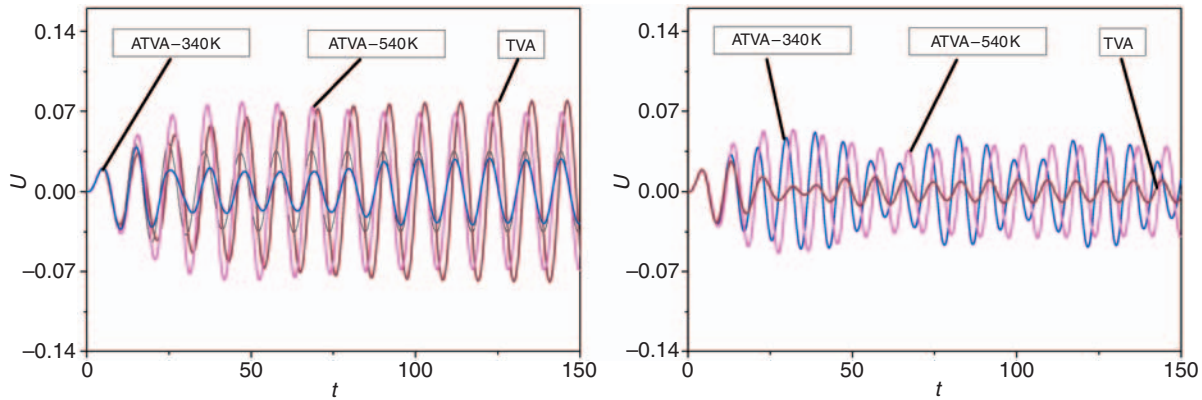


Figure 11. Primary system time response and stress–strain curve at  $T = 340$  K.



**Figure 12.** TVA and ATVA primary system time responses. Note: Left,  $\varpi = 0.58$ ; Right,  $\varpi = 0.72$ .

A more detailed analysis of the system should be considered for a proper design of the absorber. Figure 12 establishes a comparison among the displacement time history of the primary system considering three different conditions: TVA, ATVA at  $T = 540$  K and ATVA at  $T = 340$  K. Two different frequencies are of concern showing how it can change primary system vibration reduction.

The previous results can be better understood by considering the frequency domain response expressed in terms of the maximum amplitudes as a function of forcing frequency. This analysis assumes the same initial conditions for each forcing frequency:  $\{U_1, U'_1, U_2, U'_2\} = \{0, 0, 0, 0\}$ . Figure 13 shows this frequency domain response for the same results showed in Figures 10–12. It can be observed that the better performance of each absorber depends on temperature and excitation conditions. Note that the ATVA tends to present better performance but it depends on forcing characteristics since the TVA can achieve smaller primary system amplitudes responses for some forcing frequencies. Moreover, the ATVA at  $T = 340$  K presents smaller amplitudes responses for forcing frequencies around  $\varpi = 0.6$  when compared to its performance at  $T = 540$  K. This kind of behavior is due to the energy dissipation associated with hysteresis loop, which does not happen at the higher temperature. It should be highlighted that differences from the elastic TVA and the SMA–ATVA performances could be altered by temperature variations.

Different parameters are now of concern considering a higher damping coefficient ( $\xi_1 = \xi_2 = 0.2$ ). This change is related to a system modification indicating the increase of dissipation associated with other aspects different from SMA hysteretic dissipation. Figure 14 shows ATVA primary system maximum amplitudes response for  $\delta = 0.01$  and different high temperatures. The equivalent 1DOF response is plotted together allowing a comparison of the absorber effect on system dynamics. Once again, this analysis assumes the same initial

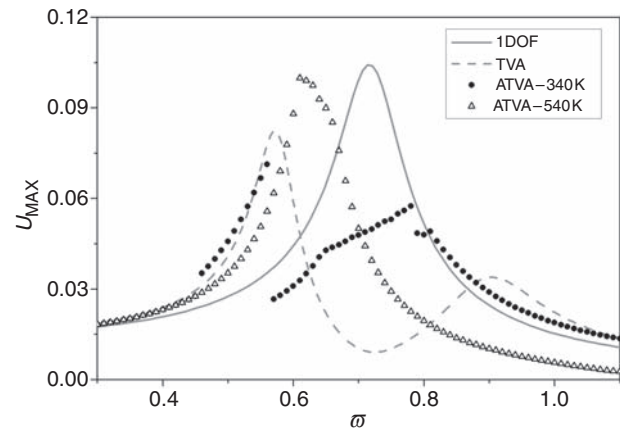


**Figure 13.** TVA and ATVA primary system maximum amplitudes response for  $\delta = 0.0075$  and  $\xi_1 = \xi_2 = 0.1$ .

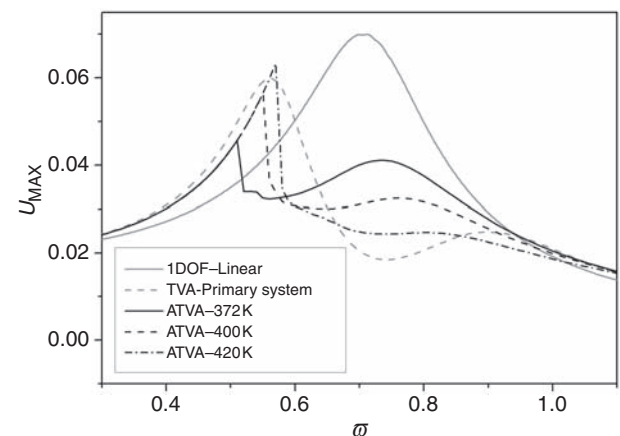


**Figure 14.** TVA and SMA–ATVA primary system maximum amplitudes response for  $\delta = 0.01$  and  $\xi_1 = \xi_2 = 0.2$ .

conditions for each forcing frequency:  $\{U_1, U'_1, U_2, U'_2\} = \{0, 0, 0, 0\}$ . It might be observed that the primary system amplitude reduction can be achieved for different forcing frequencies and different temperatures. Moreover, the system's non-linearities

introduce difficulties on the selection of the secondary system parameters; however, the temperature variation can make its application more flexible, allowing an amplitude reduction in a larger range of forcing frequencies when compared to the linear absorber.

At this point, let us try to elucidate the flexibility that SMAs can offer to the ATVA. The same parameters of the previous case is considered ( $\delta=0.01$  and  $\xi_1=\xi_2=0.2$ ). Initially, a frequency  $\varpi=0.72$  is of concern representing a resonant condition for the 1DOF oscillator. Under this condition, amplitude reductions

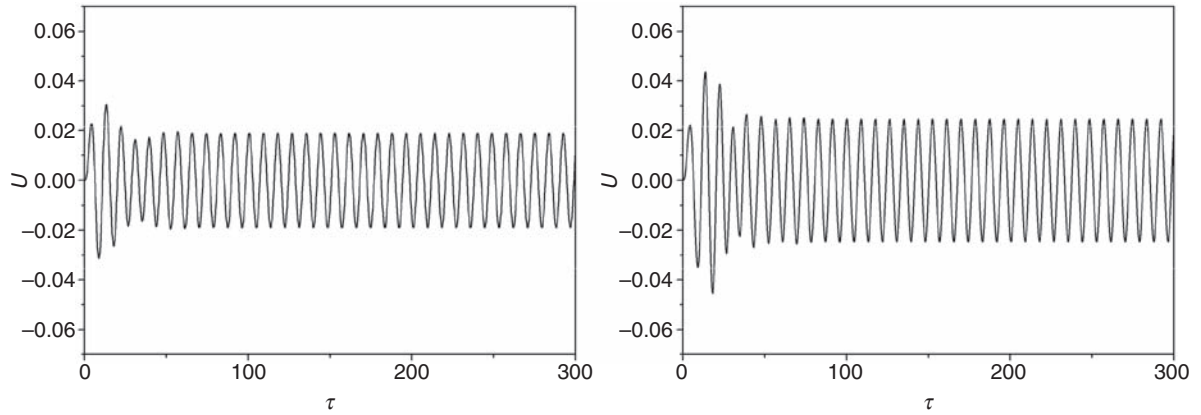


**Figure 15.** Primary system time response for  $\varpi=0.72$  ( $\delta=0.01$  and  $\xi_1=\xi_2=0.2$ ). Note: Left, TVA; Right, ATVA at  $T=420$  K.

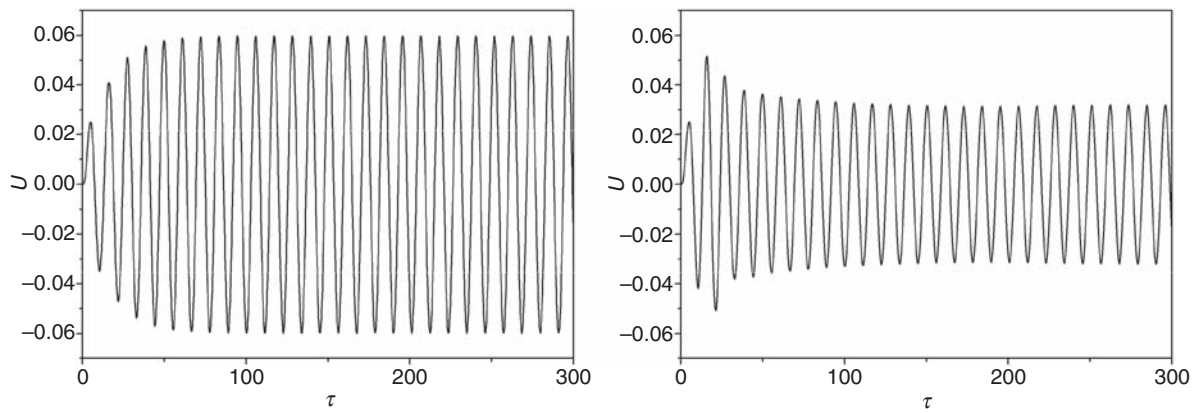


**Figure 16.** Primary system time response for  $\varpi=0.58$  ( $\delta=0.01$  and  $\xi_1=\xi_2=0.2$ ). Note: Left, TVA; Right, ATVA at  $T=372$  K.

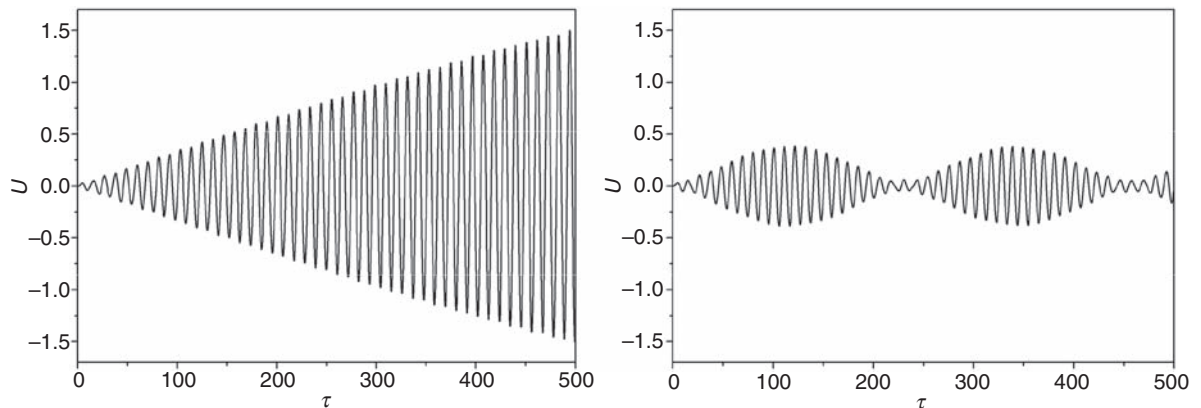


**Figure 17.** Primary system time response for  $\varpi=0.58$  ( $\delta=0.01$  and  $\xi_1=\xi_2=0$ ). Note: Left, TVA; Right, ATVA at  $T=372$  K.

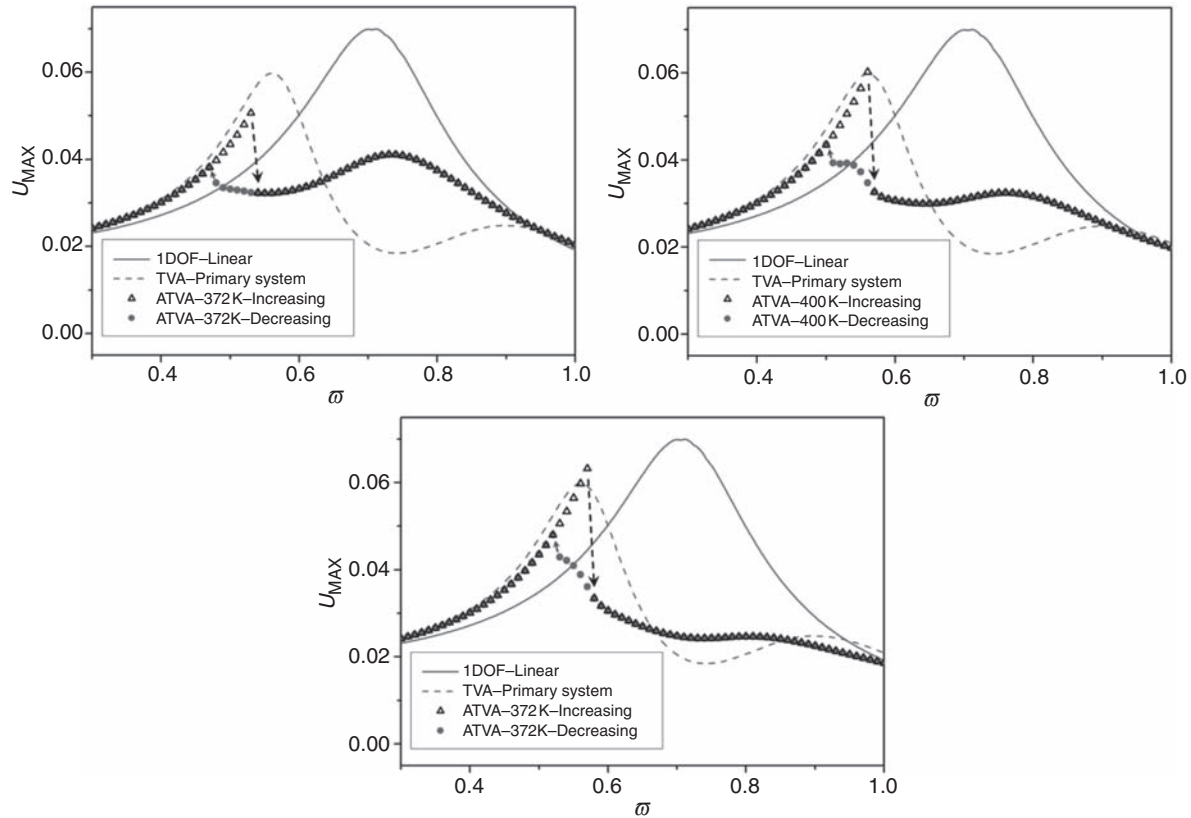


**Figure 18.** SMA–ATVA primary system maximum amplitudes response increasing (up-sweep) and decreasing (down-sweep) frequencies for  $\delta = 0.01$ ,  $\xi_1 = \xi_2 = 0.2$ , and different temperatures: 372, 400, and 420 K.

are successfully achieved by the TVA as well as by the SMA–ATVA at  $T = 420$  K (Figure 15). Nevertheless, the consideration of the vibration absorber together with the primary system represents a new 2DOF system being related to two new resonant frequencies that must be avoided. Therefore, the attachment of a linear absorber makes it possible for the system to run only in specific range of frequencies, and large variations of this frequency may be dramatic for the system response. The SMA–ATVA, however, presents hysteretic behavior together with temperature dependent properties that may change this scenario making it possible to attenuate the vibration amplitudes in these new resonant frequencies. Figure 16 shows TVA and ATVA primary system response for  $\omega = 0.58$ , where the ATVA temperature is  $T = 372$  K. The importance of this kind of flexibility is even more clear by considering an undamped system where  $\xi_1 = \xi_2 = 0$ . Under this condition, the TVA system is related to a classical resonant condition when  $\omega = 0.58$  (Figure 17, left panel). The ATVA, however, can reduce vibration amplitudes in an efficient way (Figure 17, right panel).

The analysis of dynamical jumps is essential for a proper design of related to the SMA–ATVA. This analysis is now of concern by considering the influence of forcing frequency variation on system response. Figure 18 shows the same analysis developed in

Figure 14 but now investigating increasing (up-sweep) and decreasing (down-sweep) frequencies. This figure plots together the 1DOF and the TVA responses allowing a proper comparison among all results. Note that dynamical jumps are close to the first natural frequency of the TVA system. Besides, it should be highlighted that the jump positions are altered by temperature variations.

## CONCLUSIONS

This article discusses the use of SMA elements in vibration absorbers. The thermomechanical behavior of SMAs is described by a proper constitutive model. Initially, a 1DOF oscillator is presented in which the restitution force is given by the SMA element. The analysis of this system shows that the hysteretic behavior is related to high energy dissipation, indicating the use of SMA element in a vibration absorber. The next step of this work consists in the dynamical analysis of an adaptive-passive absorber built with an SMA element (ATVA). The behavior of this system is compared with a passive absorber, composed of a linear elastic element (TVA). The TVA attenuates the primary system vibration amplitudes in a chosen forcing frequency; however, two new resonance frequencies appear and must be avoided. The SMA–ATVA is capable of reducing the system response amplitudes not only on the initially

chosen forcing frequency but also in these two new resonant frequencies that appear in the TVA. This happens as a consequence of the mechanical properties variation due to temperature-induced phase transformations and also to the energy dissipation related to the hysteretic behavior due to stress-induced phase transformation. It should be highlighted that SMA-ATVA attenuation capacity in a specific frequency can be controlled by altering the system temperature. This behavior confers flexibility to the ATVA, allowing its use in situations where excitation frequency varies. SMA actuators have a great potential to be used in vibration control, nevertheless, it is important to mention that the strong non-linear behavior of SMAs may introduce unusual, complex dynamical responses that should be further investigated during the design of the application. The parametric analysis developed in this article shows different kinds of possibilities related to the response of SMA absorbers, indicating some situations that should be investigated during the design. In this regard, it is important to mention dynamical jumps and temperature dependent behavior.

## ACKNOWLEDGMENTS

The authors would like to acknowledge the support of the Brazilian Research Agencies CNPq and FAPERJ and through the INCT-EIE (National Institute of Science and Technology – Smart Structures in Engineering) the CNPq and FAPEMIG. The Air Force Office of Scientific Research (AFOSR) is also acknowledged and it is important to mention the inspirational discussions with James M. Fillerup and Victor Giurgiutiu.

## REFERENCES

- Aguiar, R.A.A., Savi, M.A. and Pacheco, P.M.C.L. 2010. "Experimental and Numerical Investigations of Shape Memory Alloy Helical Springs," *Smart Mater. Struct.*, 19:1–9.
- Auricchio, F., Fugazza, D. and DesRoches, R. 2006. "Numerical and Experimental Evaluation of the Damping Properties Of Shape-Memory Alloys," *J. Eng. Mater. Technol. – ASME*, 128:312–319.
- Baêta-Neves, A.P., Savi, M.A. and Pacheco, P.M.C.L. 2004. "On the Fremond's Constitutive Model For Shape Memory Alloys," *Mech. Res. Commun.*, 31:677–688.
- Bernardini, D. and Rega, G. 2005. "Thermomechanical Modelling, Nonlinear Dynamics And Chaos in Shape Memory Oscillators," *Math. Comput. Modell. Dyn. Syst.*, 11:291–314.
- Brennan, M.J. 2006. "Some Recent Developments in Adaptive Tuned Vibration Absorbers/Neutralisers," *Shock Vib.*, 13:531–543.
- Elahinia, M.H., Koo, J.H. and Tan, H. 2005. "Improving Robustness of Tuned Vibration Absorbers Using Shape Memory Alloys," *Shock Vib.*, 12:349–361.
- Ibrahim, R.A. 2008. "Recent Advances in Nonlinear Passive Vibration Isolators," *J. Sound Vib.*, 314:371–452.
- Inman, D.J. 1989. *Vibration with Control, Measurement and Stability*, Prentice Hall, Englewood Cliffs.
- Lagoudas, D.C. 2008. *Shape Memory Alloys: Modeling and Engineering Applications*, Springer, New York.
- Lagoudas, D.C., Khan, M.M., Mayes, J.J. and Henderson, B.K. 2004. "Pseudoelastic SMA Spring Elements for Passive Vibration Isolation: Part II – Simulations and Experimental Correlations," *J. Intell. Mater. Syst. Struct.*, 15:443–470.
- Machado, L.G., Lagoudas, D.C. and Savi, M.A. 2009. "Lyapunov Exponents Estimation for Hysteretic Systems," *Int. J. Solids Struct.*, 46:1269–1598.
- Machado, L.G. and Savi, M.A. 2003. "Medical Applications of Shape Memory Alloys," *Braz. J. Med. Biol. Res.*, 36:683–691.
- Machado, L.G., Savi, M.A. and Pacheco, P.M.C.L. 2003. "Nonlinear Dynamics and Chaos in Coupled Shape Memory Oscillators," *Int. J. Solids Struct.*, 40:5139–5156.
- Meirovitch, L. 1986. *Elements of Vibration Analysis*, McGraw-Hill, New York.
- Monteiro Jr, P.C.C., Savi, M.A., Netto, T.A. and Pacheco, P.M.C.L. 2009. "A Phenomenological Description of the Thermomechanical Coupling and the Rate-dependent Behavior of Shape Memory Alloys," *J. Intell. Mater. Syst. Struct.*, 20:1675–1687.
- Oliveira, S.A., Savi, M.A. and Kalamkarov, A.L. 2010. "A Three-dimensional Constitutive Model for Shape Memory Alloys," *Arch. Appl. Mech.*, 80:1163–1175.
- Ortiz, M., Pinsky, P.M. and Taylor, R.L. 1983. "Operator Split Methods for the Numerical Solution of the Elastoplastic Dynamic Problem," *Comput. Methods Appl. Mech. Eng.*, 39:137–157.
- Paiva, A. and Savi, M.A. 2006. "An Overview of Constitutive Models for Shape Memory Alloys," *Math. Prob. Eng.*, 2006:1–30.
- Paiva, A., Savi, M.A., Braga, A.M.B. and Pacheco, P.M.C.L. 2005. "A Constitutive Model for Shape Memory Alloys Considering Tensile-compressive Asymmetry and Plasticity," *Int. J. Solids Struct.*, 42:3439–3457.
- Rustighi, E., Brennan, M.J. and Mace, B.R. 2005a. "A Shape Memory Alloy Adaptive Tuned Vibration Absorber: Design and Implementation," *Smart Mater. Struct.*, 14:19–28.
- Rustighi, E., Brennan, M.J. and Mace, B.R. 2005b. "Real-time Control of a Shape Memory Alloy Adaptive Tuned Vibration Absorber," *Smart Mater. Struct.*, 14:1184–1195.
- Saadat, S., Salichs, J., Noori, M., Hou, Z., Davoodi, H., Bar-On, I., Suzuki, Y. and Masuda, A. 2002. "An Overview of Vibration and Seismic Applications of NiTi Shape Memory Alloy," *Smart Mater. Struct.*, 11:218–229.
- Salichs, J., Hou, Z. and Noori, M. 2001. "Vibration Suppression of Structures Using Passive Shape Memory Alloy Energy Dissipation Devices," *J. Intell. Mater. Syst. Struct.*, 12:671–680.
- Santos, B.C. and Savi, M.A. 2009. "Nonlinear Dynamics of a Nonsmooth Shape Memory Alloy Oscillator," *Chaos, Soliton. Fract.*, 40:197–209.
- Savi, M.A. and Pacheco, P.M.C.L. 2002. "Chaos and Hyperchaos in Shape Memory Systems," *Int. J. Bifurcation Chaos*, 12:645–657.
- Savi, M.A. and Paiva, A. 2005. "Describing Internal Subloops due to Incomplete Phase Transformations in Shape Memory Alloys," *Arch. Appl. Mech.*, 74:637–647.
- Savi, M.A., Paiva, A., Baêta Neves, A.P. and Pacheco, P.M.C.L. 2002. "Phenomenological Modeling and Numerical Simulation of Shape Memory Alloys: A Thermo-plastic-phase Transformation Coupled Model," *J. Intell. Mater. Syst. Struct.*, 13:261–273.
- Savi, M.A., Sa, M.A.N., Paiva, A. and Pacheco, P.M.C.L. 2008. "Tensile-compressive Asymmetry Influence on the Shape Memory Alloy System Dynamics," *Chaos, Soliton. Fract.*, 36:828–842.
- Shaw, J.A. and Kyriakides, S. 1995. "Thermomechanical Aspects of Ni-Ti," *J. Mech. Phys. Solids*, 43:1243–1281.
- Sitnikova, E., Pavlovskaja, E. and Wiercigroch, M. 2008. "Dynamics of an Impact Oscillator with SMA Constraint," *Eur. Phys. J. Special Topics*, 165:229–238.
- Sitnikova, E., Pavlovskaja, E., Wiercigroch, M. and Savi, M.A. 2010. "Vibration Reduction of the Impact System by an SMA Restraint: Numerical Studies," *Int. J. Non linear Mech.*, 45:837–849.

- van Humbeeck, J. 2003. "Damping Capacity of Thermoelastic Martensite in Shape Memory Alloys," *J. Alloys Compd.*, 355:58–64.
- Williams, K., Chiu, G. and Bernhard, R. 2002. "Adaptive-passive Absorbers Using Shape-memory Alloys," *J. Sound Vib.*, 249:835–848.
- Williams, K., Chiu, G. and Bernhard, R. 2005. "Dynamic Modelling of a Shape Memory Alloy Adaptive Tuned Vibration Absorber," *J. Sound Vib.*, 280:211–234.
- Yoon, S.H. 2008. "Experimental Investigation of Thermo-mechanical Behaviors in Ni-Ti Shape Memory Alloy," *J. Intell. Mater. Syst. Struct.*, 19:283–289.